processes

MDPI

*Article*

# Study on the Energy Evolution and Damage Mechanism of Fractured Rock Mass Under Stress–Seepage Coupling

**Haiqing Shuang [1,2,3], Xiangxiang Liu [1,2], Bin Zhou [1,2,3,*], Liang Cheng [1,2,3,*], Haifei Lin [1,2,3], Biao Hu [1,2,3] and Zijia Liu [1,2]**

[1] College of Safety Science and Engineering, Xi'an University of Science and Technology, Xi'an 710054, China; shuanghaiqing@163.com (H.S.)
[2] Key Laboratory of Western Mine Exploitation and Hazard Prevention, Ministry of Education, Xi'an University of Science and Technology, Xi'an 710054, China
[3] Shaanxi Provincial Key Laboratory of Gas Disaster Prevention and Control in Western Coal Mines, Xi'an 710054, China
* Correspondence: zhou_bin@xust.edu.cn (B.Z.); chengliang2611@163.com (L.C.)

**Abstract:** In the process of deep mining, the dynamic disasters of coal and rock occur frequently under the action of high stress and high seepage pressure, the essence of which is energy-driven coal rock failure. In order to explore the energy evolution law and damage mechanism of sandstone with intermittent cracks under the coupling effect of stress and seepage, in this paper, by comparing the differences in mechanical characteristics between fractured rock and intact rock, the energy evolution characteristics, crack propagation, and micro-damage mechanism of fractured rock under different confining pressures and seepage pressures are analyzed. The research shows that: (1) The local stress drop phenomenon occurs in the fractured rock during the loading process, and the stress–strain shape is 'bimodal'. At the same time, there is stress concentration at both ends of the fracture. (2) The energy conversion of the fractured rock changes in stages during loading. As confining pressure rises, the energy storage limit and the maximum dissipation energy go up. The increase in seepage pressure reduces the energy storage limit, while the dissipation energy shows an upward trend. The energy consumption ratio curve shows 'concave' evolution during the loading process. (3) Based on the dissipation energy and residual stress, the damage state of the specimen is analyzed, and the proposed damage variable can reasonably explain the whole process of the damage evolution of intermittent fractured rock under stress and seepage. (4) The increase in confining pressure increases the friction between the particles inside the sample and promotes the transformation of the sample from tensile failure to shear failure. The seepage pressure reduces the friction between the particles in the sample through the air wedge effect to deepen the damage degree, thus promoting the tensile failure of the sample.

**Keywords:** stress–seepage coupling; intermittent fissure; energy evolution; damage characteristics



Academic Editor: Qingbang Meng

Received: 3 January 2025
Revised: 14 January 2025
Accepted: 16 January 2025
Published: 18 January 2025

**Citation:** Shuang, H.; Liu, X.; Zhou, B.; Cheng, L.; Lin, H.; Hu, B.; Liu, Z. Study on the Energy Evolution and Damage Mechanism of Fractured Rock Mass Under Stress–Seepage Coupling. *Processes* **2025**, *13*, 270. https://doi.org/10.3390/pr13010270



## 1. Introduction

With the depletion of shallow coal seam resources and the increase in mining intensity, coal mining is gradually shifting to the deep [1,2]. In the process of deep mining, the coupling effect of high ground stress and seepage pressure on the deformation of rock mass is more and more significant, which leads to the aggravation of construction difficulty. Meanwhile, water also has a certain deteriorating effect on rocks, which contributes to

a decrease in strength parameters. A large number of engineering practices show that the leading role of cracks in rock mass in the failure process of deep confining pressure is gradually enhanced [3–5].

Under the mutual influence of the stress field and seepage field, the mechanical properties and failure modes of fractured rock mass are more complicated [6]. According to thermodynamics, rock failure is the deformation and instability driven by energy. The energy evolution law and damage characteristics of deep fractured rock mass under stress–seepage coupling are revealed from the perspective of energy, which is closer to the essence of rock failure under load. It has important theoretical significance and practical value for the prevention and control of rock mass disasters under the influence of mining. Therefore, it is necessary to carry out research on the energy evolution law of fractured rock mass under complex stress states [7–9].

In the study of rock energy evolution, many scholars have carried out in-depth research. The research results mainly focus on two aspects: one is the analysis of energy based on experiments, and the other is the study of energy evolution theory based on numerical simulation. In the aspect of experimental research, the constitutive relation between energy dissipation and rock mass failure is analyzed or the failure model of rock mass structure is established to judge the failure condition of rock mass [10]. Starting from the stress loading path, Li et al. analyzed the energy evolution characteristics of coal and rock masses with different height ratios under different stress paths and proposed the concept of the energy dissipation ratio [11]. Xue [12], Li [13], and Peng [14] et al. carried out a triaxial compression test on deep coal–rock and analyzed the influence of different confining pressures on the energy evolution characteristics of coal–rock in the process of failure. Miao [15], Wang [16], and Wang [17] et al. explored the energy dissipation and energy conversion mode of coal–rock in the process of cyclic loading and unloading and unearthed the damage mechanism of coal–rock in terms of energy. Based on the cyclic loading and unloading of coal and rock, Wu [18] et al. considered the influence of the fracture angle on energy during rock failure according to the change in coal seam stress. Chu [19] et al. studied the energy evolution characteristics of coal–rock under different loading and unloading rates. Zhou [20] and Fu [21] et al. modified coal–rock damage variables based on dissipated energy and established the relationship between coal–rock permeability and energy damage variables. Li et al. established a coal damage constitutive model from the perspective of energy dissipation based on statistical damage theory [22]. Liu et al. established a segmented constitutive model for the deformation of yellow sandstone under uniaxial compression based on the theory of dissipative energy evolution, using the Logistic function combined with damage mechanics theory and effective medium theory [23]. Guo et al. established a generalized strength criterion for rock failure mechanisms based on energy conservation and elastic strain energy [24].

In terms of numerical simulation, Yu [25], Wang [26], and Wang [27] et al. used PFC 2D to explore the failure characteristics of rocks with different fracture dip angles and fracture lengths under different confining pressures and explained the energy conversion mechanism. Wong [28] used Ansys Autodyn to simulate the merging process of coplanar cracks in rock during compression and identified crack types by analyzing crack development. Zhang et al. used UDEC-Trigon to establish uniaxial compression and Brazilian splitting models to analyze the influence of the coal–rock height ratio on the failure mode of the coal–rock combination [29]. Chen et al. derived a new rock failure criterion based on the law of conservation of energy and related mechanical parameters [30].

In summary, lots of scholars have made some achievements in the study of energy evolution and damage characteristics in the process of the deformation of coal and rock mass. However, in previous studies, most scholars focused on the mechanical behavior of

rock under a single stress or seepage condition while ignoring the interaction between the two. During the deep mining process, rock is often subjected to the dual effects of stress and seepage at the same time. The coupling effect of stress–seepage will greatly change the mechanical properties and energy evolution trend of rock. There are few studies on the energy evolution and damage characteristics of fractured rock mass under the influence of complex stress coupling factors such as different confining pressures and seepage pressures. At the same time, in fractured rock, the existence of a rock bridge has an effect on the stress and deformation of rock mass [31]. Based on this, this paper focuses on intermittent fractured rock and conducts triaxial compression tests under different confining pressures and seepage pressures. The mechanical properties, energy evolution characteristics, and damage characteristics of fractured rock mass under stress–seepage coupling are analyzed. The research contents of energy evolution characteristics and damage characteristics of fractured rock under the coupling influence of complex factors are enriched so as to provide a reference for underground engineering safety problems such as deep mining and tunnel excavation.

## 2. Material and Methods

### 2.1. Sample Preparation

The rock used in this experiment was taken from the sandstone in the Jinjiang area of Chongqing. In order to explore the energy evolution and damage characteristics of fractured rock under stress–seepage coupling, in this paper, a double parallel fracture with an intermittent fracture angle of 50°, a fracture spacing of 20 mm, a fracture length of 10 mm, and a rock bridge angle of 90° were designed.

### 2.2. Test Equipment

In this experiment, the self-developed thermal fluid–solid coupling triaxial seepage test system for gas-bearing coal and rock developed by Chongqing University was used (Figure 1). The maximum axial pressure of the equipment is 500 MPa, the maximum confining pressure is 60 MPa, and the maximum seepage pressure is 6 MPa. The deformation measurement includes axial deformation and radial deformation. The allowable maximum axial displacement is 60 mm, and the maximum radial displacement is 6 mm. The measurement accuracy range of axial pressure and confining pressure is ±1%. During the test, the relevant parameters such as axial pressure, confining pressure, seepage pressure, axial deformation, and radial deformation can be dynamically monitored in real time.

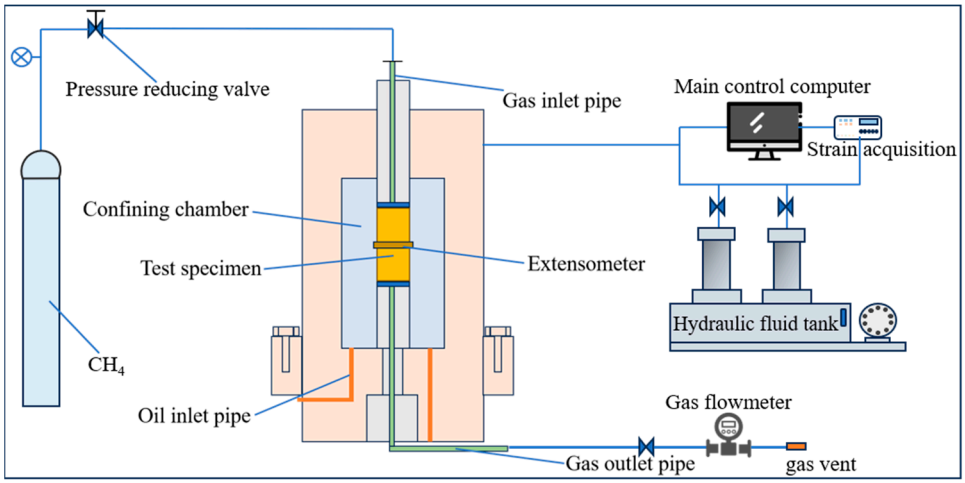


**Figure 1.** Test equipment.

### 2.3. Experimental Procedures

In order to better restore the occurrence state of deep rock mass, this paper sets different confining pressures and seepage pressures to simulate the low-, medium-, and high-stress complex environment of deep rock mass. As we know, there is a well-established relationship between vertical stress and burial depth, which serves as a crucial reference for our experimental design.

$$\sigma_v = 0.0271H \quad (1)$$

Drawing on the established findings of previous classical research regarding in situ stress, it can be deduced that when the confining pressure reaches 5 MPa, the corresponding depth of the rock layer is approximately 185 m; at a confining pressure of 7.5 MPa, the relevant rock layer is situated at around 277 m; and when the confining pressure is set at 10 MPa, the approximate depth of the rock layer is 369 m. Based on these theoretical deductions, triaxial compression–seepage tests were carried out under confining pressures of 5 MPa, 7.5 MPa, and 10 MPa and seepage pressures of 1 MPa, 2 MPa, and 3 MPa (Table 1). The loading path is shown in Figure 2, and the specific steps are as follows.

**Table 1.** Experimental plan.

| Test Scheme | Fracture Angle | Loading Speed | Confining Pressure (MPa) | Seepage Pressure (MPa) |
|---|---|---|---|---|
| 1 | 50° | 0.025 mm/min | 5.0 | 1.0 |
| 2 | | | | 2.0 |
| 3 | | | | 3.0 |
| 4 | 50° | 0.025 mm/min | 7.5 | 1.0 |
| 5 | | | | 2.0 |
| 6 | | | | 3.0 |
| 7 | 50° | 0.025 mm/min | 10.0 | 1.0 |
| 8 | | | | 2.0 |
| 9 | | | | 3.0 |

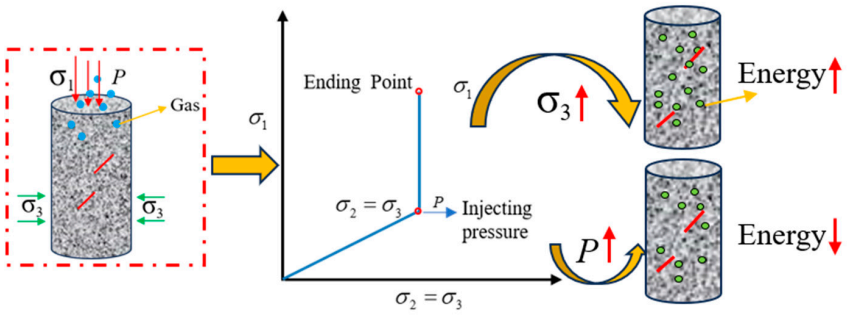


**Figure 2.** Stress loading path.

(1) The test piece was installed, and the test piece was clamped with a heat-shrinkable pipe. The heat-shrinkable pipe was uniformly attached to the sample by an electric blow, and the upper and lower sections were clamped with a metal hoop.

(2) The test conditions were adjusted, and the axial pressure and confining pressure were gradually applied to the hydrostatic pressure state of 5 MPa. Then, the seepage pressure was gradually applied to 1 MPa, and the axial pressure was always greater than the confining pressure during the loading process.

(3) After the stress loading, the seepage pressure and confining pressure were stable. The loading speed was 0.025 mm/min until the specimen was destroyed.

(4) By repeating the above steps, the triaxial seepage tests under confining pressures of 7.5 MPa and 10 MPa and seepage pressures of 2 MPa and 3 MPa were carried out.

### *2.4. Energy Evolution Theory in Triaxial Compression*

Based on the law of conservation of energy and the relationship of function transformation, when a rock sample is subjected to external load, it undergoes compaction, elastic deformation, plastic deformation, and failure stages. Each stage is accompanied by energy conversion, which is essentially the result of energy distribution. Xie et al. [7] pointed out that the deformation and failure process of rock samples is caused by energy accumulation and dissipation from the perspective of energy evolution. Therefore, based on the energy theory, this paper analyzes the deformation and failure characteristics of rock samples with intermittent fractures under the coupling of stress and seepage and reveals the deformation and failure mechanism of rock samples with intermittent fractures.

Figure 3 shows the calculation diagram of typical dissipated energy and elastic energy. The shadow area is the elastic energy stored in the rock. And the region enclosed by the stress–strain curve and the unloading curve corresponds to the dissipated energy of the rock. It is assumed that the rock specimen always has no heat exchange with the outside during the loading process. The total energy $U$ is generated by the external force on the rock sample.

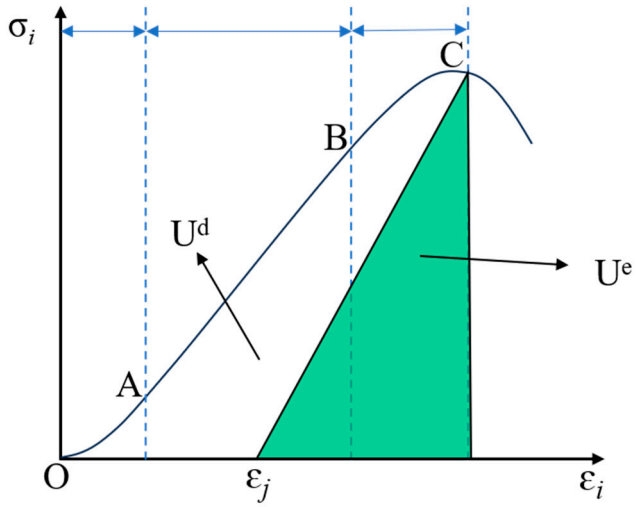


**Figure 3.** Relationship between dissipated energy and elastic energy in a stress–strain curve.

According to the first law of thermodynamics,

$$U = U^e + U^d \tag{2}$$

where $U^e$ is the elastic energy that can be released by the rock and $U^d$ is the dissipated energy during loading. In the complex stress state, the total energy, elastic energy, and dissipative energy of a rock sample can be expressed in the principal stress space by the following formula:

$$U = U^e + U^d = \int \sigma_1 d\varepsilon_1 + \int \sigma_2 d\varepsilon_2 + \int \sigma_3 d\varepsilon_3 \tag{3}$$

$$U^e = \frac{1}{2E}[\sigma_1^2 + \sigma_2^2 + \sigma_3^2 - 2\nu(\sigma_1\sigma_2 + \sigma_2\sigma_3 + \sigma_1\sigma_3)] \tag{4}$$

where $\sigma_1$, $\sigma_2$, and $\sigma_3$ are, respectively, the maximum, middle, and minimum principal stresses, $\varepsilon_1$, $\varepsilon_2$, and $\varepsilon_3$ are the strains generated in the corresponding directions of the three principal stresses, respectively, $E$ is the elastic modulus, and $\nu$ is Poisson's ratio.

In the triaxial test, $\sigma_2 = \sigma_3$, and the formula is rewritten as:

$$U = U^d + U^e = \int \sigma_1 d\varepsilon_1 + 2\int \sigma_3 d\varepsilon_3 \tag{5}$$

$$U^e = \frac{1}{2E}[\sigma_1^2 + 2\sigma_3^2 - 2\nu(2\sigma_1\sigma_3 + \sigma_3^2)] \tag{6}$$

The analysis of radial elastic energy is based on the related literature. During the loading process, the elastic energy produced by axial deformation is much larger than that produced by radial deformation [12,32,33]. It is considered that the radial elastic energy is neglected, so it can be simplified as:

$$U^e = \frac{\sigma_1^2}{2E} \tag{7}$$

The dissipation energy calculation formula of the joint Formulas (2) and (7) is as follows:

$$U^d = U - U^e = U - \frac{\sigma_1^2}{2E} \tag{8}$$

## 3. Results and Analysis

### *3.1. Stress–Strain Behavior*

The compression failure process of rock can usually be divided into four stages: compaction stage, elastic deformation stage, plastic deformation stage, and post-peak failure stage. Figure 4 shows the stress–strain curves of the intact and intermittent fractured rock under the coupling of stress and seepage.

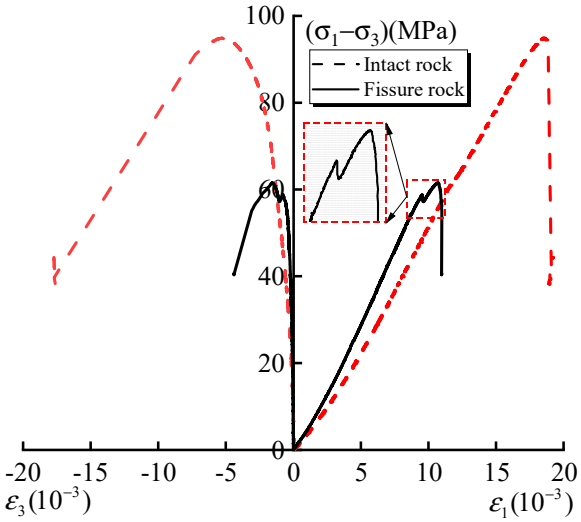


**Figure 4.** Stress–strain curves of the intact rock and fractured rock.

It can be seen from the figure that the full stress–strain process of the intact rock samples and intermittent fractured rock samples is similar under different confining pressures and seepage pressures. In the compaction stage, the original micropores inside the rock are gradually sealed under the action of external pressure. The stress–strain curve is concave, and the concave shape produced by the intact rock is relatively obvious. In the stage of elastic deformation, the micro-cracks of rock mass are further compressed and closed, and the stress–strain curve is approximately linear. In this paper, the elastic modulus of the intermittent fractured rock is 5.79 GPa, which is significantly higher than that of the intact rock at 4.98 GPa. In the stage of plastic deformation, secondary cracks are generated inside the rock, and irreversible plastic deformation occurs. After entering the peak failure

stage, the bearing capacity of the sample reaches the limit and failure occurs, and the peak strength and strain of the fractured rock are much smaller than those of the intact rock.

The peak strength and peak strain of the intact rock are 94.8 MPa and 18.5 × $10^{-3}$, respectively, while the peak strength and strain of the intermittent fractured rock are 61.5 MPa and 10.7 × $10^{-3}$, respectively.

Different from the complete rock sample, the stress local drop phenomenon occurs in the rock with intermittent cracks, and the stress–strain curve shows a 'bimodal' shape. The analysis shows that the existence of intermittent cracks makes the load unable to be transmitted through the prefabricated cracks, resulting in stress concentration at both ends of the cracks. The crack tip easily initiates micro-cracks. With the stress loading to a certain extent, the crack tip ruptures and initiates cracks, and the strength of the sample decreases, which shows that the stress–strain curve falls. At this time, the broken main crack and the insufficiently developed crack form the shear interlocking effect, which makes the bearing capacity of the specimen rise again until the peak stress is reached. The crack is connected with the prefabricated crack and is fully developed. The specimen loses its bearing capacity, and the stress–strain curve decreases instantaneously. It is worth noting that the second growth rate of the stress–strain curve is lower than the first growth rate.

In order to further explore the influence of confining pressure and seepage pressure on the intermittent fractured rock, Figures 5 and 6 show the stress–strain curves of the intermittent fractured rock under different confining pressures and seepage pressures. It can be seen from Figure 5 that under the condition of low confining pressure (confining pressure of 5 MPa), the first stress drop in the fracture sample appears after the stress peak point, and with the increase in confining pressure, the stress drop appears before the peak value. The peak stress and peak strain increase with the increase in confining pressure, and the stress–strain curve is steeper with the increase in confining pressure.

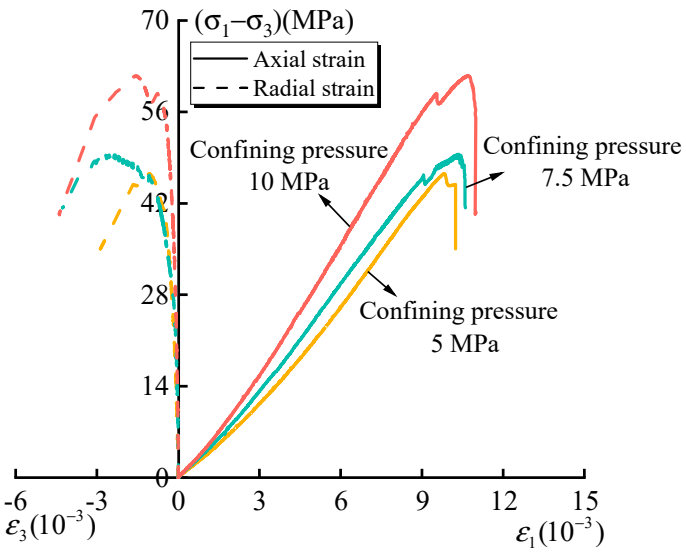


**Figure 5.** Different confining pressure stress–strain curves of fractured rock.

The analysis shows that the existence of confining pressure plays a role in compaction constraint on the primary micro-cracks inside the specimen. The higher the confining pressure is, the more difficult the crack is to expand. The shear interlocking effect between the crack that is not fully expanded at the tip of the cracked specimen and the main crack is more obvious, so the secondary bearing capacity of the specimen is higher. At the same time, with the increase in confining pressure, the internal ductility of the fractured specimen is enhanced and the bearing capacity is improved. When the confining pressure

increases from 5 MPa to 7.5 MPa and 10 MPa, the peak stress increases by 6.4% and 32.2%, respectively, and the peak axial strain increases by 5.6% and 9.2%, respectively.

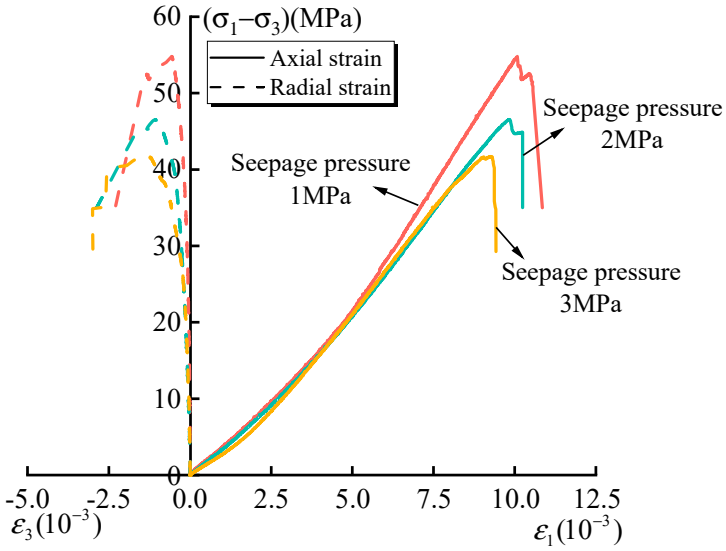


**Figure 6.** Different pressure stress–strain curves of fractured rock.

Figure 6 shows the stress–strain curves of the intermittent fractured rock under different seepage pressure conditions. It can be seen from the figure that the peak stress and the peak strain of the fractured specimen decrease with the increase in seepage pressure. At the same time, with the increase in seepage pressure, the secondary bearing capacity of fractured specimens decreases after the first drop of stress. The analysis shows that the permeable gas has a deterioration effect on the fracture sample, promotes crack propagation at the crack tip of the sample, weakens the shear interlocking effect between the fracture surfaces, and makes the fracture sample more easily damaged. For example, when the seepage pressure increases from 1 MPa to 2 MPa and 3 MPa, the peak stress of the rock samples decreases by 18.1% and 23.8%, respectively, and the peak radial deformation increases by 85% and 138%.

In summary, due to the change in the internal crack structure of the fractured rock specimen, under the action of an external load, the main crack at the crack tip forms a shear interlocking effect with the under-developed crack, which makes the stress–strain curve of the fractured specimen bimodal. With the increase in confining pressure, the shear interlocking effect is enhanced, and the increase in seepage pressure will weaken the shear interlocking effect and reduce the compressive strength of the sample.

### *3.2. Energy Evolution Characteristics*

#### 3.2.1. Energy Evolution Law

Based on the above energy calculation method, the energy evolution characteristic curves of fractured rock samples under different confining pressures and seepage pressures during loading were obtained. Due to limited space, the energy variation law of the intermittent fractured rock under different confining pressures and seepage pressures is similar. This paper only shows the energy evolution characteristics under the condition of a constant confining pressure of 5 MPa and a constant pressure of 2 MPa.

It can be seen from Figures 7 and 8 that the total energy, elastic energy, and dissipation energy curves of the fractured rock increase with the increase in stress and strain under different confining pressures and seepage pressures. In the initial compaction stage, the work of the external force is mainly turned into dissipated energy from closing the rock's internal primary micro-fractures, and there is basically no energy storage. The energy

evolution curves of the three are basically coincident. In Figure 7a, for example, when the stress is loaded to 3.6 MPa, the difference between the elastic energy and the dissipated energy is only 0.0001 MJ·m$^{-3}$. With the increase in axial stress, the growth rate of elastic energy rises gradually, while that of dissipated energy remains largely unchanged. The energy absorbed by the rock samples is mainly converted into elastic energy. In the stage of plastic deformation, new cracks are generated and expanded inside the rock sample, and the growth rate of dissipated energy is gradually accelerated. When approaching the peak stress, the growth rate of elastic energy begins to slow down, while the growth rate of dissipated energy gradually accelerates. The elastic energy curve decreases in a cliff-like manner, and the proportion of elastic energy decreases rapidly.

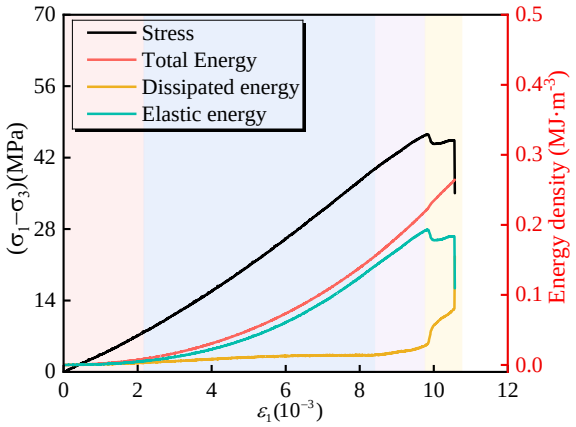


(**a**) Confining pressure 5 MPa

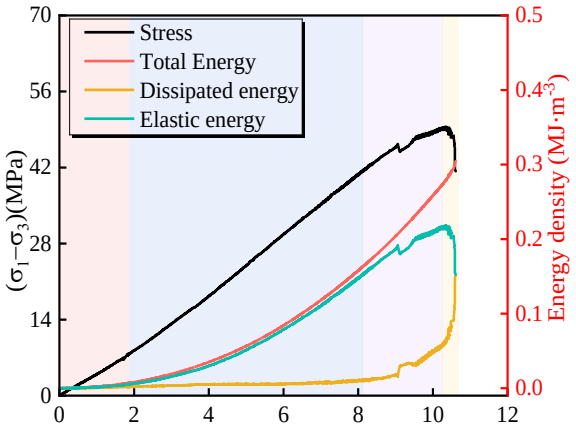


(**b**) Confining pressure 7.5 MPa

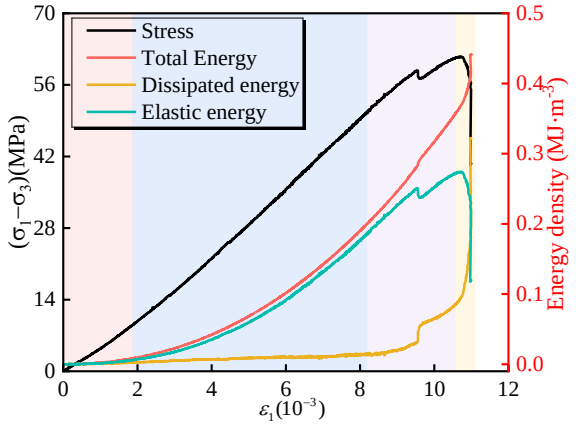


(**c**) Confining pressure 10 MPa

**Figure 7.** Stress–strain–energy evolution curves under different confining pressure conditions.

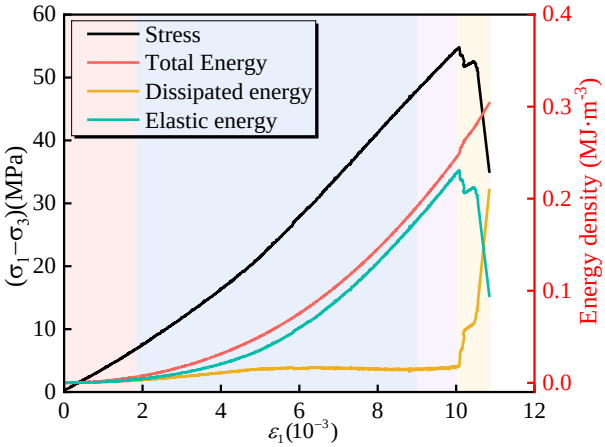


(**a**) Seepage pressure 1 MPa

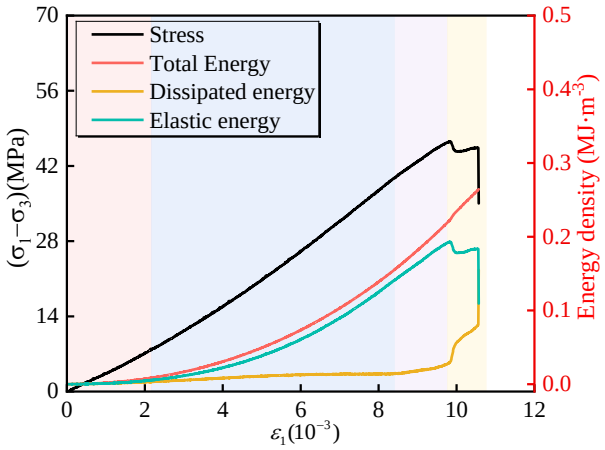


(**b**) Seepage pressure 2 MPa

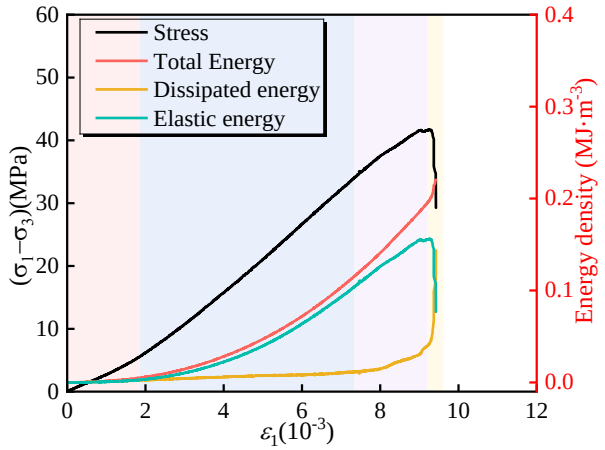


(**c**) Seepage pressure 3 MPa

**Figure 8.** Stress–strain–energy evolution curves under different pressure conditions.

During the loading process, the elastic energy appears as the local drop phenomenon, while the dissipation energy appears as the local 'sudden increase' phenomenon. From the above analysis, the stress concentration phenomenon at the crack tip can be seen. As the crack spreads, the energy amassed at its tip is released instantly, causing the dissipated energy to rise and the elastic energy to drop instantaneously. The shear interlocking effect between cracks makes the energy carried by the sample increase twice.

Figure 9 shows the variation trend in elastic energy and dissipation energy with confining pressure and seepage pressure after the first drop in stress. From Figure 9a, it can be seen that when the elastic energy falls for the first time, the secondary load-bearing

elastic energy and the dissipated energy consumed by the sample damage increase with the increase in confining pressure. The released energy grows with the rise in confining pressure. For example, when the confining pressure increases from 5 MPa to 10 MPa, the elastic energy and dissipation energy increase from 0.006 and 0.017 MJ·m$^{-3}$ to 0.037 and 0.036 MJ·m$^{-3}$, respectively.

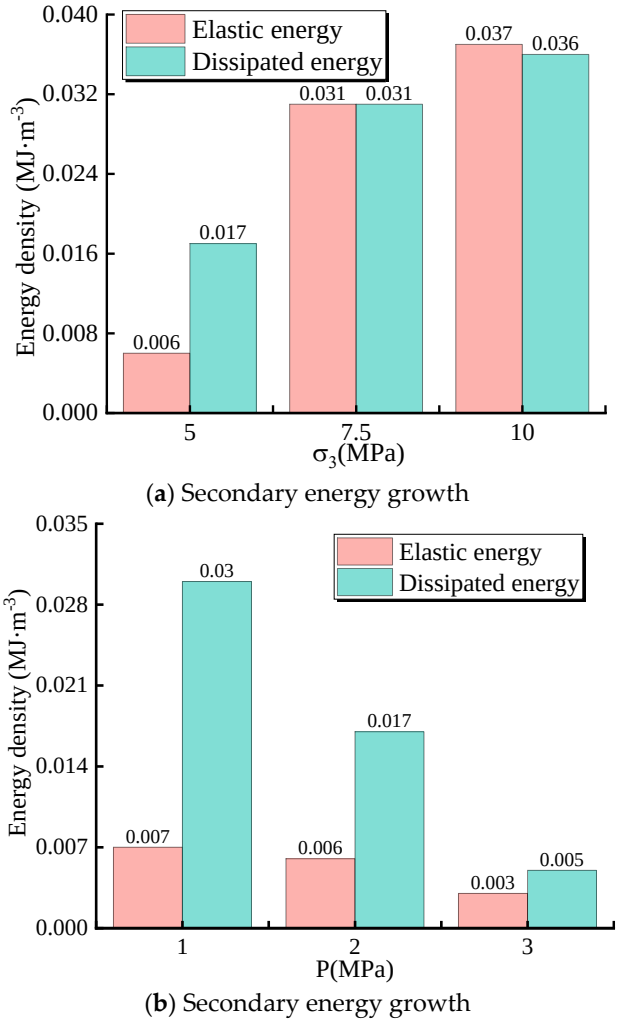


**Figure 9.** Relationship of energy secondary growth–confining pressure–permeability pressure.

On the contrary, it can be seen from Figure 9b that the secondary load-bearing elastic energy and the dissipated energy consumed by sample damage decrease with the increase in seepage pressure under different seepage pressure conditions. For example, when the seepage pressure increases from 1 MPa to 3 MPa, the elastic energy and dissipation energy decrease from 0.007 MJ·m$^{-3}$ and 0.03 MJ·m$^{-3}$ to 0.003 MJ·m$^{-3}$ and 0.005 MJ·m$^{-3}$, respectively.

In order to further quantitatively describe the influence of confining pressure and seepage pressure on rock energy evolution, the characteristic energy parameters of rock the mass energy storage limit $U^e_{\max}$ and the maximum dissipation energy density $U^d_{\max}$ are introduced to describe the features of rock energy change. The peak limit value of the elastic energy density is the energy storage limit of rock, which is used to characterize the ability of rock to accumulate elastic deformation energy. The greater the energy storage limit of rock, the stronger the deformation resistance. The peak limit of dissipation energy density is defined as the maximum dissipation energy density, which has the ability to

characterize the energy dissipation of rock. The larger the maximum dissipated energy density, the more damage cracks accumulate in the rock, and the closer the rock is to failure.

It can be seen from Figures 10 and 11 that under different pressure conditions, the increase in confining pressure causes different degrees of increase in the energy storage limit and maximum dissipation energy of the rock samples. At the initial stage (confining pressure of 5 MPa), the energy storage limit and the maximum dissipation energy of the rock samples are 0.23 MJ·m$^{-3}$ and 0.014 MJ·m$^{-3}$, respectively, when the seepage pressure is 1 MPa. When the confining pressure rises to 7.5 MPa and 10 MPa, the energy storage limit and the maximum dissipation energy increase by 0.08% and 250% and by 30% and 314%, respectively. When the seepage pressure is 2 MPa and 3 MPa, it shows the same properties as the seepage pressure of 1 MPa. It is shown that the energy absorbed by the rock mass under high confining pressure is greater than that under low confining pressure. The higher the confining pressure, the stronger the anti-deformation energy of the sample, the greater the energy consumed by the destruction, and the less likely it is to be destroyed.

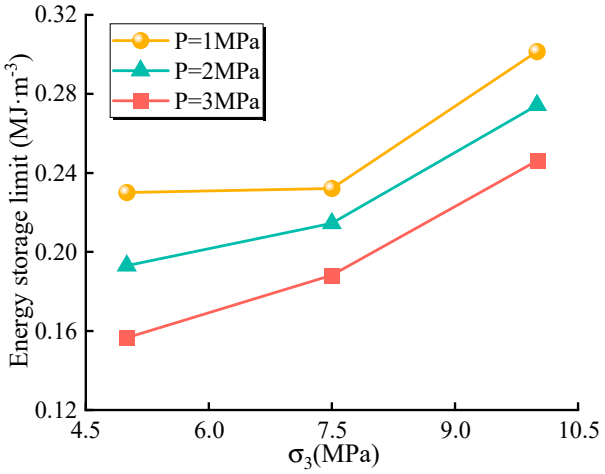


**Figure 10.** Relationship between energy storage limit and confining pressure under different pressure conditions.

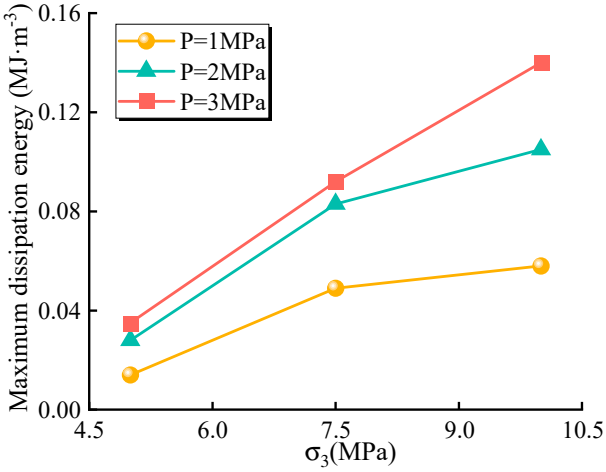


**Figure 11.** Relationship between maximum dissipated energy and confining pressure under different pressure conditions.

Figures 12 and 13 show the relationship between the energy storage limit and the maximum dissipation energy of the rock samples under different confining pressures and the change in seepage pressure. It can be seen from the figure that the energy storage limit of the rock samples declines as the seepage pressure increases. The difference is that the

maximum dissipation energy goes up along with the rise in seepage pressure. The main reason is that the increase in seepage pressure weakens the force between the particles in the rock sample, which aggravates the damage degree of the sample and causes an increase in dissipation energy. At the initial stage (seepage pressure of 1 MPa), the energy storage limit and the maximum dissipated energy of the sample were 0.23 MJ·m$^{-3}$ and 0.014 MJ·m$^{-3}$, respectively. When the seepage pressure increased to 2 MPa and 3 MPa, the energy storage limit decreased by 17% and 34%, respectively, and the maximum dissipation energy increased by 100% and 150%, respectively.

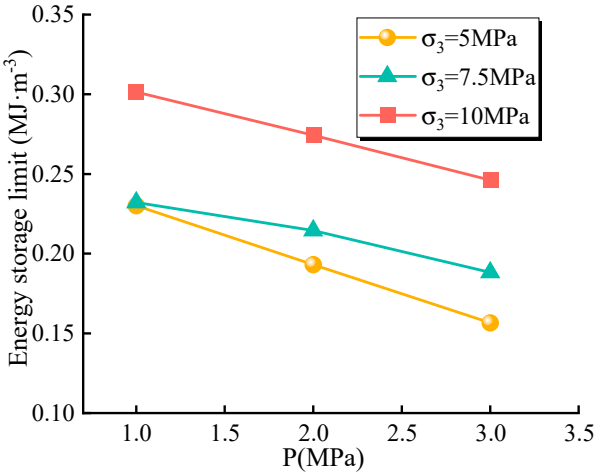


**Figure 12.** Relationship between limit energy storage and pressure under different confining pressure conditions.

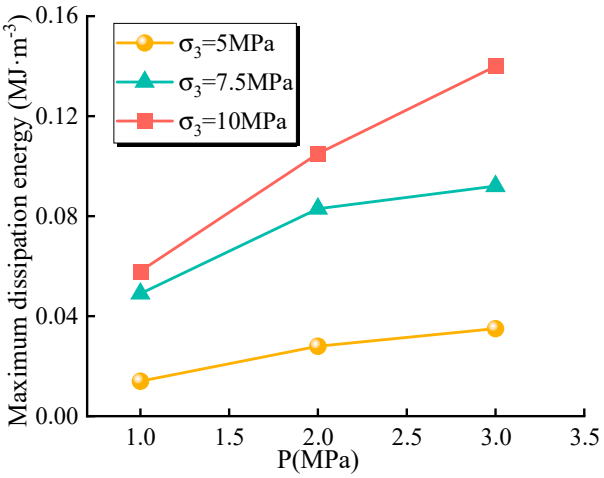


**Figure 13.** Relationship between maximum dissipated energy and pressure under different confining pressures.

Considering the interaction between confining pressure and seepage pressure, the limit surface relations of maximum dissipation energy and energy storage are drawn, respectively, as shown in Figures 14 and 15. Based on linear fitting, the surface relationship is fitted as follows:

$$U^{e}_{\max} = 0.012\sigma_3 - 0.042P + 0.001\sigma_3 P + 0.19 \quad R^2 = 0.89 \tag{9}$$

$$U^{d}_{\max} = 0.002\sigma_3 - 0.021P + 0.006\sigma_3 P + 0.003 \quad R^2 = 0.95 \tag{10}$$

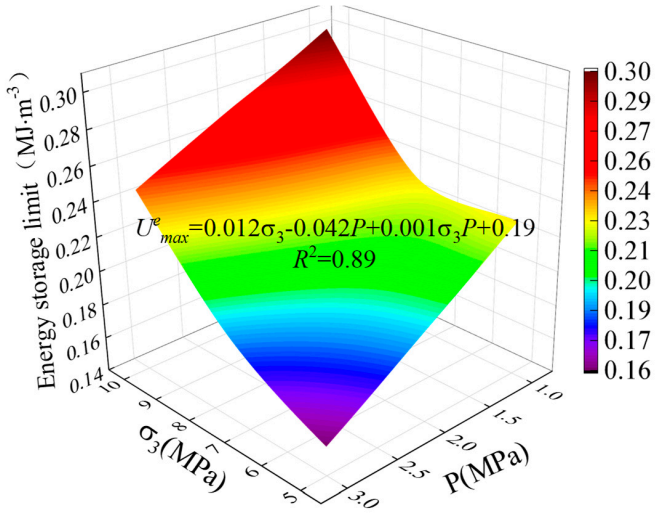


**Figure 14.** Surface diagram of energy storage limit–confining pressure–pressure.

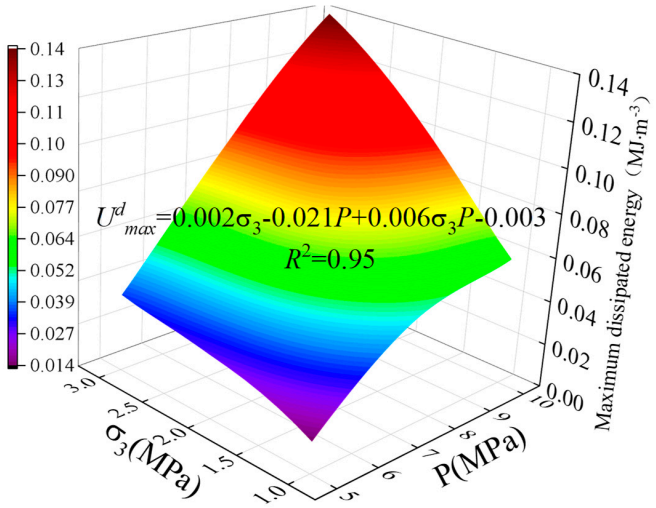


**Figure 15.** Surface diagram of maximum dissipated energy–confining permeability–pressure.

The fitting correlation coefficients were 0.95 and 0.89, respectively, indicating a relatively high fitting degree. The analysis shows that the linear expression of the maximum dissipated energy and energy storage limit has high accuracy.

### 3.2.2. Energy Distribution Law

Relevant studies have shown that the accumulation of dissipative energy is the main factor leading to rock failure. For rock samples, the process from complete state loading to failure is the result of internal damage accumulation. It is also the process of energy conversion mutation inside a rock sample, and the dissipated energy can indirectly reflect the irreversible plastic deformation inside a rock sample [34]. Therefore, the energy consumption ratio is introduced to characterize the cumulative results of the internal damage of the rock samples during loading and then reflect the stable state of the rock samples. The energy consumption ratio is calculated as follows:

$$k = \frac{U^d}{U^e} \tag{11}$$

where $U^d$ is the dissipative energy of the rock sample and $U^e$ is the elastic energy of the rock sample.

From Figures 16 and 17 and Table 2, it can be seen that during the loading and failure process of the rock samples, the energy consumption ratio curve is 'concave', showing the distribution characteristics of 'high at both ends and low in the middle'. The energy consumption ratio of the rock samples at the initial loading stage is $k > 1$. The main reason is that the primary micro-fractures inside the rock sample are closed under the action of external force, and the dissipation energy is dominant in this process. According to the above energy evolution characteristic curve, although dissipated energy is the main energy in this stage, the total amount of energy is small. With the increase in axial stress, the energy consumption ratio shows a downward trend $k < 1$. The main reason is that in this process, the work of the external force is mainly converted into elastic energy, and the proportion of elastic energy continues to rise, so the energy consumption ratio $k$ shows a downward trend. There is an 'inflection point' before the peak, that is, the energy consumption ratio is the lowest. When the stress is higher than the corresponding stress at this point, the energy consumption ratio of the loaded rock mass begins to rise. The reason is that when the energy consumption ratio reaches the lowest point, under the action of external force, a large number of micro-cracks propagate and the rock samples converge at the same time, and large plastic deformation occurs. The dissipation energy begins to grow rapidly, and its growth rate is gradually higher than the elastic energy growth rate, so the energy consumption ratio begins to rise. Upon reaching peak stress, the elastic energy nosedives while the dissipated energy spikes, making the energy consumption ratio 'jump'.

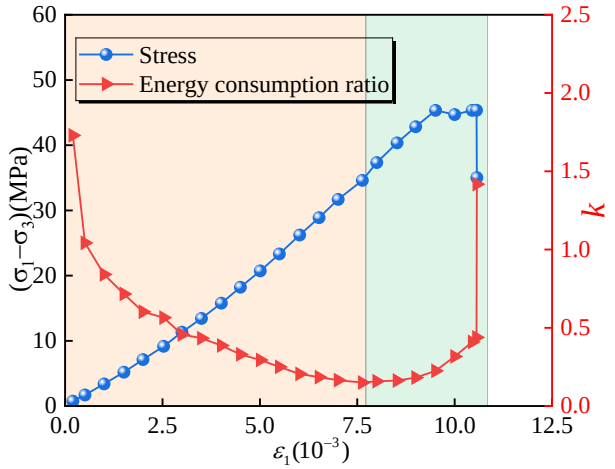


(**a**) Confining pressure 5 MPa

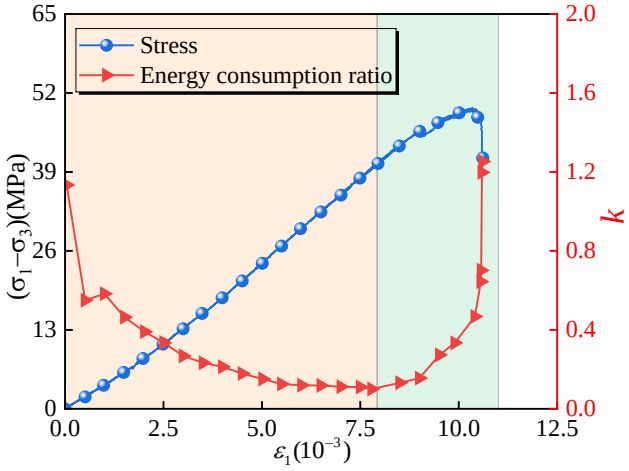


(**b**) Confining pressure 7.5 MPa

**Figure 16.** *Cont.*

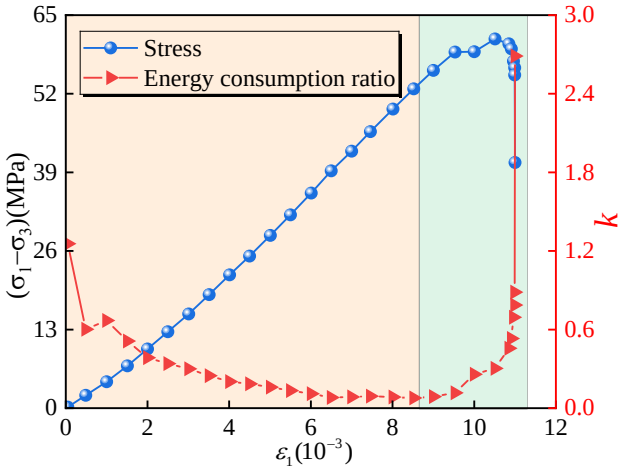


(**c**) Confining pressure 10 MPa

**Figure 16.** Stress–strain–energy consumption ratio curves under different confining pressures.

**Table 2.** Inflection point of the energy consumption ratio.

| Test Scheme | Fracture Angle | Confining Pressure (MPa) | Seepage Pressure (MPa) | The Inflection Point of the Energy Consumption Ratio |
|---|---|---|---|---|
| 1 | 50° | 5.0 | 1.0 | $8.06 \times 10^{-3}$ |
| 2 | | | 2.0 | $7.63 \times 10^{-3}$ |
| 3 | | | 3.0 | $7.12 \times 10^{-3}$ |
| 4 | 50° | 5 | 2.0 | $7.63 \times 10^{-3}$ |
| 5 | | 7.5 | | $7.79 \times 10^{-3}$ |
| 6 | | 10 | | $8.52 \times 10^{-3}$ |

Under the same seepage pressure, the 'inflection point' of the energy consumption ratio gradually moves backward with the increase in confining pressure. As shown in Figure 16, when the confining pressure increases from 5 MPa to 7.5 MPa and 10 MPa, the inflection point of the energy consumption ratio moves from $7.63 \times 10^{-3}$ to $7.79 \times 10^{-3}$ and $8.52 \times 10^{-3}$, respectively. The change in the 'inflection point' of the energy consumption ratio is related to the mechanism of brittle-to-plastic transformation with the increase in confining pressure. When the confining pressure is low, the loaded rock sample is prone to brittle failure, and the dissipation energy increases rapidly, so the inflection point of energy consumption appears earlier. With the increase in confining pressure, the protective effect of confining pressure on the rock samples inhibits the intensity of the plastic deformation of the loaded rock samples, which transforms some brittle failure of the samples into plastic failure. To a certain extent, this inhibits the speed of energy dissipation and release during rock failure, resulting in a slight delay in the inflection point of the energy consumption ratio.

Under the same confining pressure, the higher the seepage pressure, the earlier the 'inflection point' appears. As shown in Figure 17, when the seepage pressure increases from 1 MPa to 2 MPa and 3 MPa, the 'inflection point' of the energy consumption ratio moves from $8.06 \times 10^{-3}$ to $7.63 \times 10^{-3}$ and $7.12 \times 10^{-3}$, respectively. The main reason is that the gas acts on the crack tip of the rock sample, promotes the development and expansion of the crack, and has a deterioration effect on the rock sample.

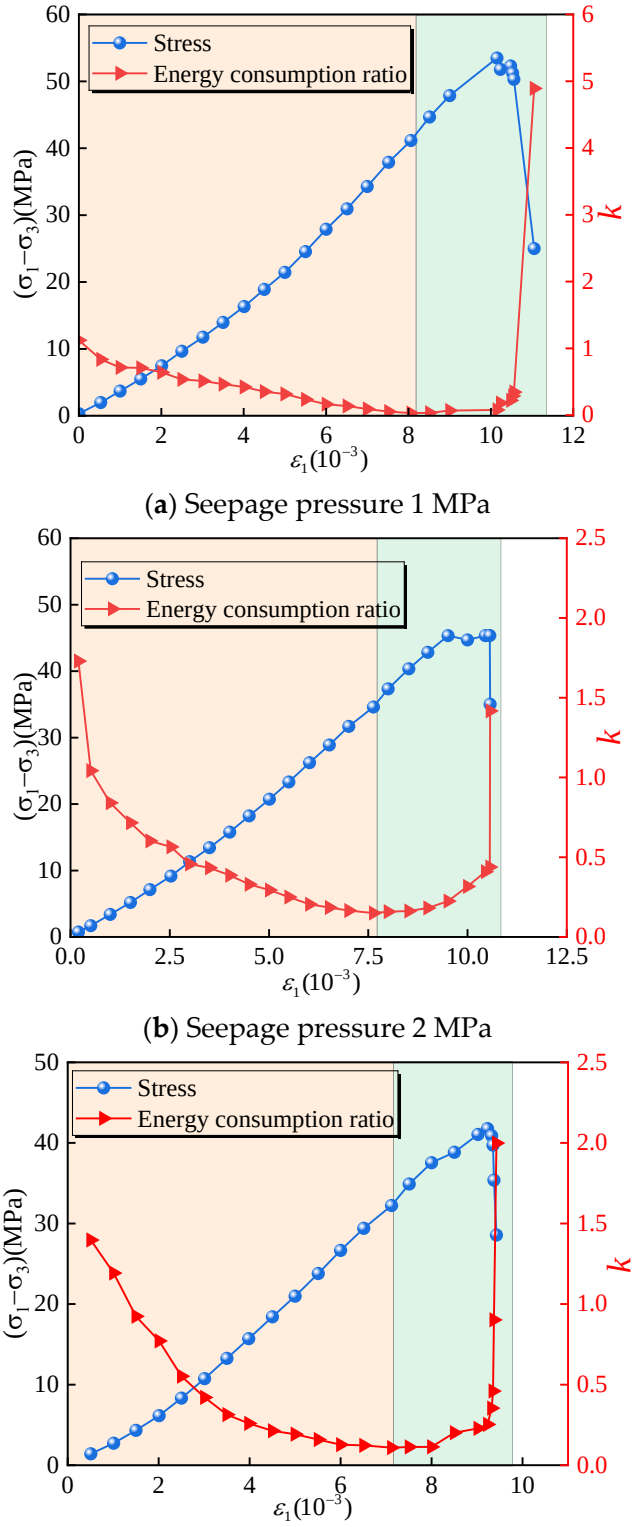


**Figure 17.** Stress–strain–energy consumption ratio curves under different pressure conditions.

With the increase in seepage pressure, the intensity of the plastic deformation of the loaded rock sample is aggravated, and part of the plastic failure is transformed into brittle failure, which increases the conversion of internal energy to dissipative energy. The deterioration effect is more significant, thereby reducing the strength of the rock itself, and the energy consumption appears earlier than the 'inflection point'.

## 4. Discussion

### 4.1. Damage Characteristics

The deformation and failure of rock is a process of gradual deterioration. For intermittent fracture specimens, the existence of cracks leads to the weakening of the internal friction of specimens. Driven by external energy, cracks continue to appear, develop, and expand, resulting in the destruction of the macroscopic rock structure [35]. It is generally believed that energy dissipation is directly related to its internal damage. The damage generated during rock deformation can be regarded as continuous energy dissipation. An increase in cumulative dissipated energy indicates that the degree of the internal damage of rock is deepening [36].

In order to quantitatively describe the damage degree of intermittent fracture specimens under the combined effect of coupling confining pressure and seepage pressure, Chen et al. proposed the rock damage variable $D$ based on dissipated energy [37], which is calculated as follows:

$$D = \frac{U^d}{U_p^d} \tag{12}$$

where $U^d$ is the energy dissipation of the sample under load and $U_p^d$ is the energy dissipation at peak load. When $D$ = 0, it means that the rock has no damage; when $D$ = 1, it means that the rock sample is damaged and the stress reaches the peak.

At the same time, it is considered that the sample has a certain bearing capacity after failure. The correction coefficient related to residual strength is introduced to rewrite the formula as follows [24]:

$$D = (1 - \frac{\sigma_r}{\sigma_c})\frac{U^d}{U_p^d} \tag{13}$$

where $\sigma_r$ is the residual stress and $\sigma_c$ is the peak stress.

According to the generalized Hooker theorem and Lemaitre strain equivalence principle, the constitutive relationship between rock damage and stress–strain can be obtained as follows:

$$\sigma = (1 - D)E\varepsilon \tag{14}$$

Substituting Equation (11) into Equation (13), the damage constitutive relation of rock based on dissipated energy can be obtained as follows:

$$\sigma = \left[1 - (1 - \frac{\sigma_r}{\sigma_c})\frac{U^d}{U_p^d}\right]E\varepsilon \tag{15}$$

According to the damage variable expression (12) and the dissipation energy damage constitutive relation (15), the damage variables and axial stresses of the samples under different confining pressures and seepage pressures were calculated and fitted, as shown in Figures 18 and 19.

It can be seen from the figures that the damage characteristics of the samples under different confining pressures and seepage pressure test conditions are basically similar. At the initial stage of loading, the energy consumed by the original cracks and micropore pressure sealing in the sample is very small, and the plastic deformation is small, so the damage variable is small. As the stress gradually increases, the energy absorbed by the rock sample is mostly converted into elastic energy stored inside it. The deformation is mainly elastic deformation. The plastic deformation caused by energy dissipation begins to appear and slowly increases. Therefore, the damage quantitative development of the rock samples shows a slow upward trend. When the stress is loaded to a certain extent, a large number of cracks expand and penetrate to consume a large amount of dissipated energy, and the

plastic deformation begins to increase rapidly. The damage variable increases greatly, and there is a 'steep increase' phenomenon. Comparing the damage evolution law of samples under different confining pressures, it can be seen that the lower the confining pressure is, the more intense the damage variable evolution of the sample is, and the growth rate is higher than that under the condition of higher confining pressure.

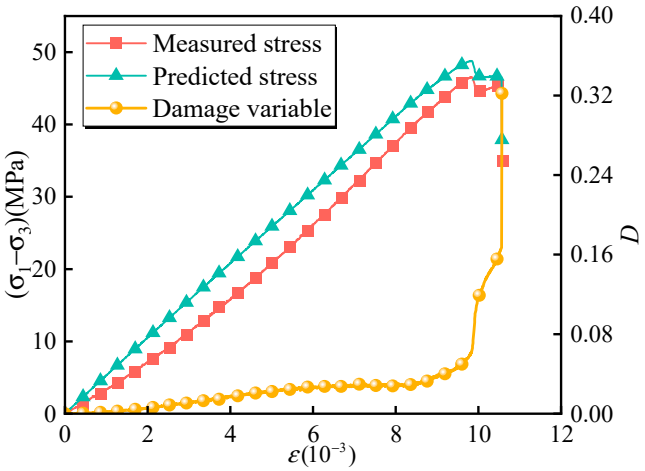


(**a**) Confining pressure 5 MPa

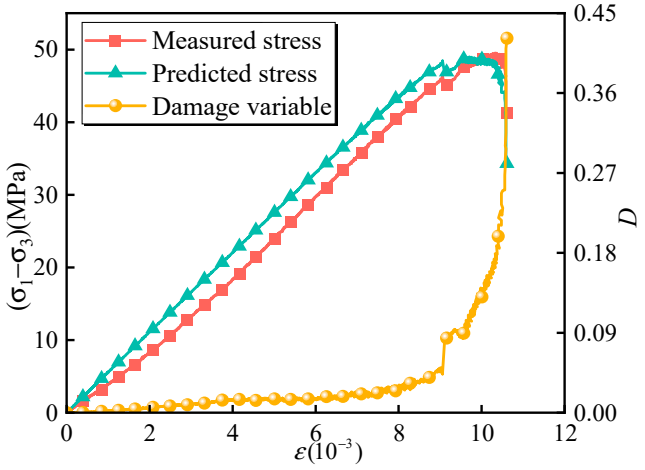


(**b**) Confining pressure 7.5 MPa

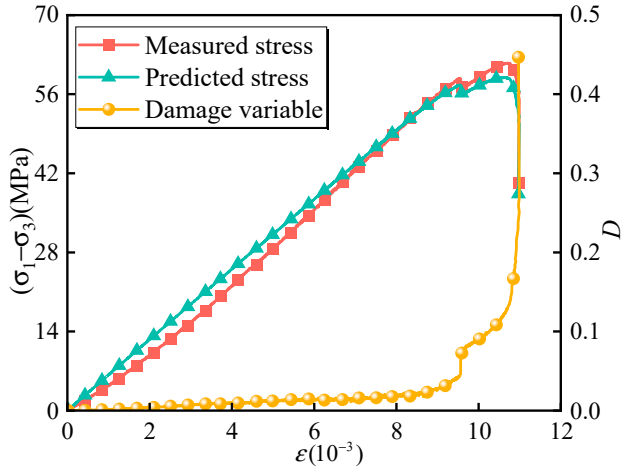


(**c**) Confining pressure 10 MPa

**Figure 18.** Different confining pressure test results and fitting curve.

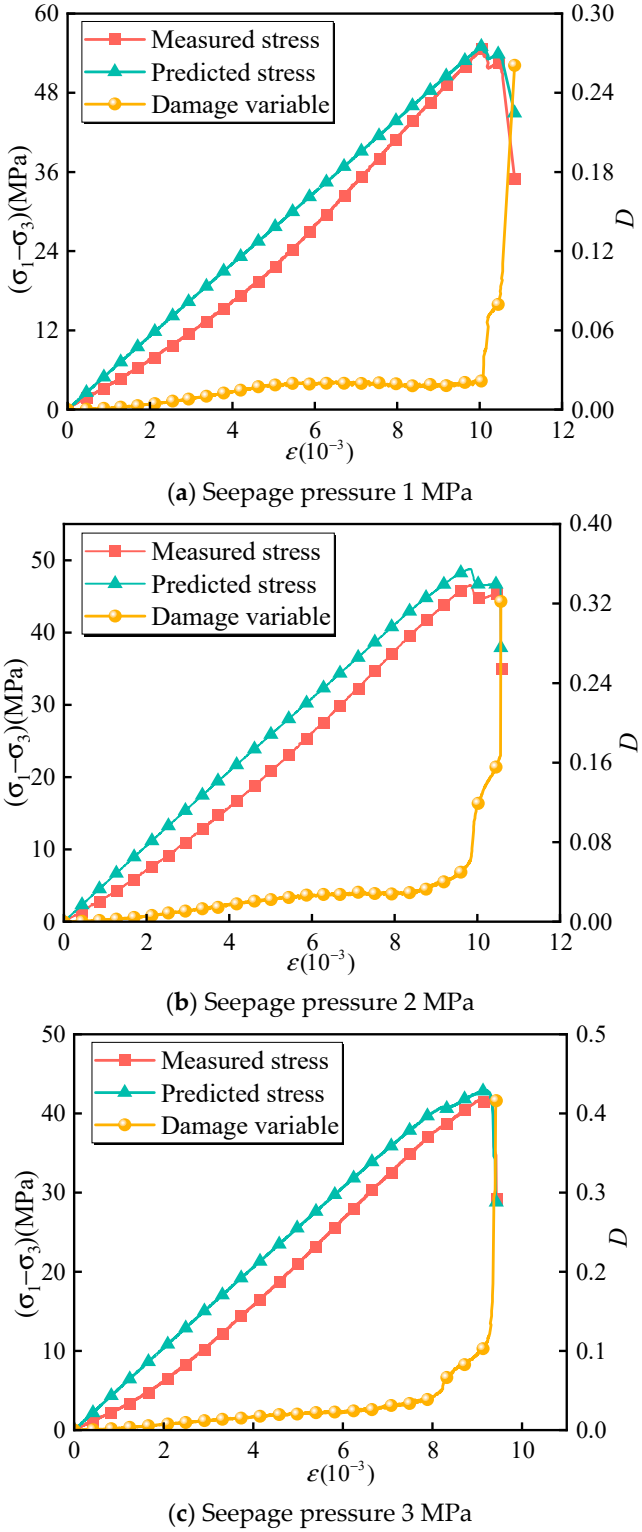


**Figure 19.** Different pressure test results and fitting curves.

Under different seepage pressure conditions, the higher the seepage pressure, the more severe the damage variable evolution. At the same time, it can be found that the curve based on dissipated energy and combined with residual stress characteristics has a higher degree of matching with the measured stress. It shows that the damage variable and damage constitutive equation based on dissipation energy can accurately describe the damage evolution process of intermittent fractured rock under different confining pressures and seepage pressures.

*4.2. Damage Mechanism*

It is concluded that the particle structure and pore network structure of the rock samples are changed under the combined action of stress–seepage. This is manifested as inhibiting or promoting the propagation of internal cracks in the rock samples. For the intermittent fractured rock, due to its special fracture structure, the crack propagation is different from that of the intact rock. Figure 20 shows the crack propagation morphology of the intermittent fractured rock. Under the action of external load, the stress concentration takes place at the tip of the crack at both ends (regions 1, 2, 3, and 4 in the figure). It may increase the local brittleness of the sample. Then, a brittle fracture occurs at the tip of the crack. The crack propagates along the crack tip to the upper and lower parts of the sample. Until the rock bridge is connected, the crack extends to the upper and lower or side boundaries of the sample, and the sample is destroyed.

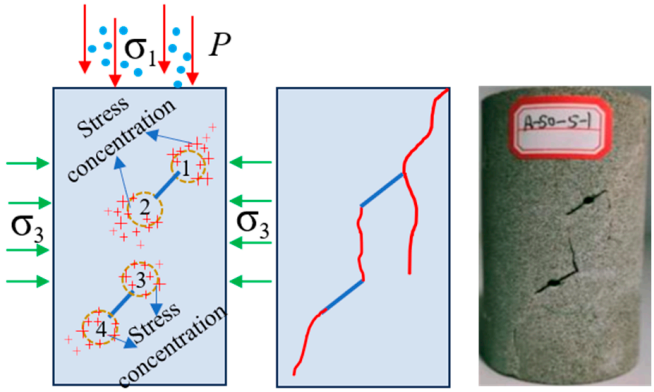


**Figure 20.** Crack propagation of intermittent fractured rock.

From the perspective of crack propagation, the existence of confining pressure will inhibit the development of tensile cracks and promote the propagation of shear cracks. As a result, the failure mode of the sample transitions from tensile failure to shear failure. On the contrary, the seepage pressure promotes the development of tensile cracks, as shown in Figures 21 and 22.

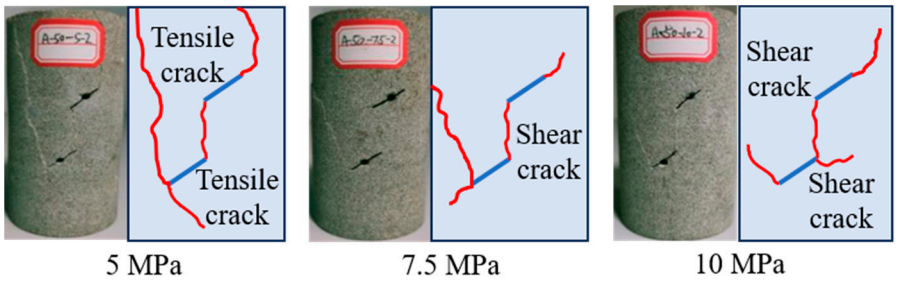


**Figure 21.** Crack morphology under different confining pressures.

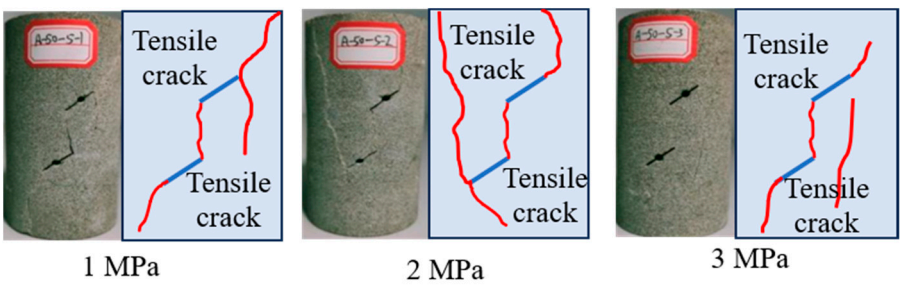


**Figure 22.** Crack morphology under different pressures.

It is generally believed that the failure of rock is mainly shear failure. Under the condition of low confining pressure, the crack propagation of rock containing cracks is always parallel to the direction of the maximum principal stress, resulting in longitudinal tensile failure. With the increase in confining pressure, the development of tensile cracks is limited, so that the cracks propagate along the direction of prefabricated cracks and shear failure occurs. With the increase in seepage pressure, the transformation of some shear cracks to tensile cracks is promoted. In the research conducted by Wang [38] and Chen [39] et al., it was observed that as confining pressure increases, the axial tensile propensity is subdued, thereby impeding the development of tensile cracks. Simultaneously, the axial compressive inclination becomes more prominent, enhancing the likelihood of shear cracks emerging and propagating along prefabricated cracks [40]. This finding aligns with the trends identified in our study.

In order to further reveal the microscopic influence mechanism of confining pressure on the fracture samples, it is assumed that the rock material is mainly composed of a variety of different sizes and different shapes of mineral particles bonded to each other. The influence of confining pressure on the fracture sample is mainly reflected in the internal friction and pore closure of the sample. Figure 23 shows a schematic diagram of the microscopic damage mechanism of the specimen under stress–seepage coupling. The crack propagation in the specimen is caused by the dislocation slip of the skeleton and mineral particles under external load. This staggered slip results in friction. With the increase in confining pressure $\sigma_3$, the contact area and contact force between the particles in the sample increase accordingly. The internal friction force of the sample increases from $f_1$ to $f_2$, and the increase in the internal friction force $f$ of the sample increases the stored energy from $U$ to $U + \Delta U$. The increase in stored energy $U$ makes it show higher bearing capacity and deformation resistance.

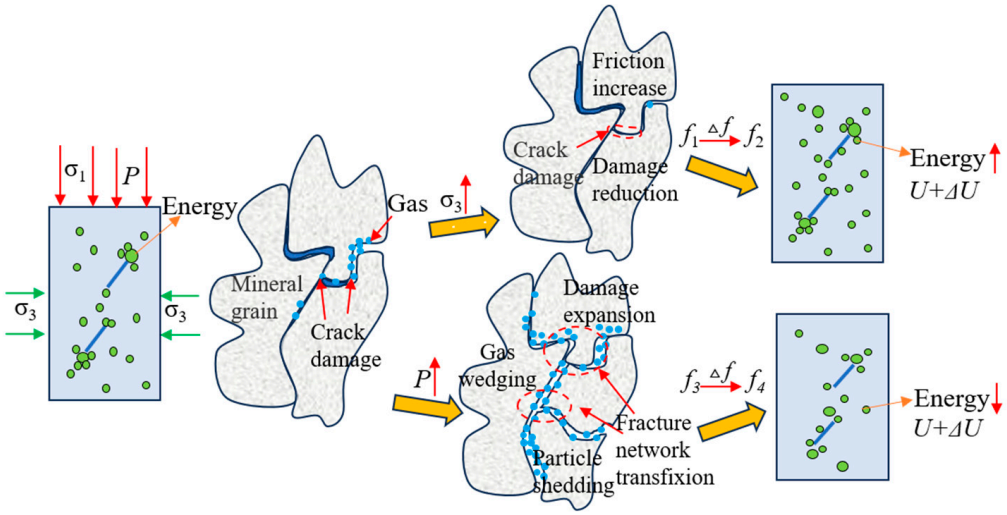


**Figure 23.** The microscopic damage mechanism of a specimen under the confining pressure–permeability coupling effect.

The results show that the influence of seepage pressure $P$ on crack propagation and penetration is mainly determined by the external stress σ and seepage pressure $P$. The existence of seepage pressure $P$ causes additional expansion stress in the rock sample, resulting in a tensile stress zone at the crack tip (Figure 24) [38]. According to the fracture theory, the effect of seepage pressure $P$ is equivalent to the tensile stress acting on the strength of rock. If the tensile stress generated at the crack tip of the specimen exceeds its tensile strength, the crack will expand and extend. The compressive strength of the sample is much higher than the tensile strength. Under the action of the seepage pressure,

the friction force between the particles in the sample decreases, resulting in loose particles or shedding of the connection between the particles. A new crack network is generated, which aggravates the crack propagation of the sample.

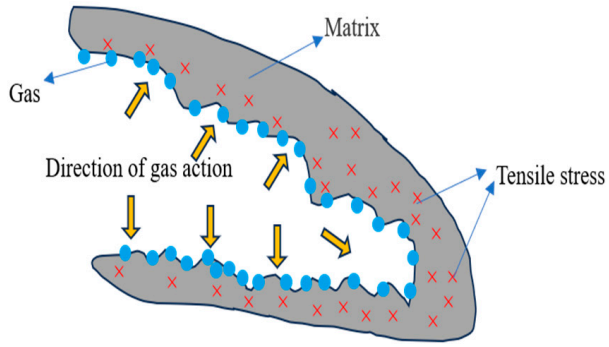


**Figure 24.** Gas wedge effect at the crack tip.

Under the influence of the above effects, combined with the Griffith theory, it can be seen that as the seepage pressure $P$ increases, the energy $U$ that the sample can store decreases to $U - \Delta U$. The energy required for crack propagation, extension, and penetration in the specimen is reduced, which makes the specimen more prone to failure.

## 5. Conclusions

In this paper, triaxial compression tests were carried out on sandstone samples with intermittent cracks under different confining pressures and seepage pressure coupling. The effects of confining pressure and seepage pressure on the mechanical properties, energy evolution, and damage characteristics of the rock samples were studied, and the conclusions are as follows:

(1) Under the coupling effect of stress and seepage pressure, due to the special fracture structure of intermittent fractured rock, the main crack at the tip of the crack is not fully developed with the crack to form a shear interlocking effect. The stress–strain curve is 'bimodal', and stress concentration occurs at both ends of the crack.

(2) The energy evolution law of intermittent fractured rock is basically the same under different confining pressures and seepage pressures. With an increase in confining pressure, the energy storage limit of rock samples increases, and more dissipation energy is generated when the samples are destroyed. An increase in seepage pressure will aggravate the crushing degree of rock samples, reduce the energy storage limit of rock, and cause an increase in dissipation energy.

(3) Under different confining pressure and seepage pressure conditions, the energy consumption ratio curve of rock decreases first and then increases, which is approximately a 'concave' evolution trend. The lowest point of the energy consumption ratio moves backward with an increase in confining pressure and advances with an increase in seepage pressure.

(4) Combined with previous studies, a stress–damage constitutive model based on dissipation energy and residual stress is modified. By comparing with the experimental data, it can be seen that the proposed model can reasonably explain the whole process of damage evolution of intermittent fractured rock under the action of stress seepage pressure.

(5) An increase in confining pressure can increase the friction force of particles inside a sample so that the failure crack morphology of the sample changes from tensile crack to shear crack. An increase in seepage pressure will promote the development of cracks into tensile cracks, which will eventually lead to tensile failure.

**Author Contributions:** H.S.: validation, resources, supervision, project administration, and review and editing; X.L.: validation, data analysis, and writing; B.Z.: data curation, review and editing, supervision, resources, and validation; L.C.: investigation and data curation; H.L.: project administration and investigation; B.H.: investigation and data curation; Z.L.: review and editing. All authors have read and agreed to the published version of the manuscript.

**Funding:** This work was supported by the National Key Research and Development Program of China (2023YFC3009001); the National Natural Science Foundation of China (52074217, 52204240); the Natural Science Foundation of Shaanxi Provincial Department of Education (2022JQ-365); the Special Foundation of Shaanxi Provincial Department of Education Science and Technology (22JK0460); and the China Postdoctoral Science Foundation Funded Project (2022MD72383).

**Data Availability Statement:** The original contributions presented in this study are included in the article. Further inquiries can be directed to the corresponding authors.

**Conflicts of Interest:** The authors declare that they have no known competing financial interests or personal relationships that could have appeared to influence the work reported in this paper.

## References

1. Jia, Z.; Xie, H.; Zhang, R.; Li, C.; Wang, M.; Gao, M.; Zhang, Z.; Zhang, Z. Acoustic Emission Characteristics and Damage Evolution of Coal at Different Depths Under Triaxial Compression. *Rock Mech. Rock Eng.* **2020**, *53*, 2063–2076. [CrossRef]
2. Zhang, X.; Tang, J.; Pan, Y.; Yu, H. Experimental study on intensity and energy evolution of deep coal and gas outburst. *Fuel.* **2022**, *324*, 124484. [CrossRef]
3. Skrzypkowski, K.; Zagórski, K.; Zagórska, A. Determination of the Extent of the rock destruction Zones around a gasification Channel on the basis of Strength Tests of Sandstone and Claystone Samples Heated at High Temperatures up to 1200 C and Exposed to Water. *Energies* **2021**, *14*, 6464. [CrossRef]
4. Xiao, P.; Li, D.; Zhao, G.; Liu, H. New criterion for the spalling failure of deep rock engineering based on energy release. *Int. J. Rock Mech. Min. Sci.* **2021**, *148*, 104943. [CrossRef]
5. Li, K.S.; Luan, Y.; Yang, S.; Liu, C. An experimental investigation on the failure behavior of sandstone with filled fissure under triaxial multilevel cyclic loading. *Fatigue Fract. Eng. Mater. Struct.* **2024**, *47*, 3375–3391. [CrossRef]
6. Liu, X.; Wang, X.; Wang, E.; Kong, X.; Zhang, C.; Liu, S.; Zhao, E. Effects of gas pressure on bursting liability of coal under uniaxial conditions. *J. Nat. Gas Sci. Eng.* **2017**, *39*, 90–100. [CrossRef]
7. Xie, H.; Li, L.; Peng, R.; Jv, Y. Energy analysis and criteria for structural failure of rocks. *J. Rock Mech. Geotech. Eng.* **2009**, *1*, 11–20. [CrossRef]
8. Chen, L. Reaserch on the Energy System of Deep Granite Considering the Stored Energy and Dissipated Energy Characteristics. Ph.D. Thesis, University of Science and Technology Beijing, Beijing, China, 2019.
9. Gao, L.; Gao, F.; Zhang, Z.; Xing, Y. Research on the energy evolution characteristics and the failure intensity of rocks. *Int. J. Min. Sci. Technol.* **2020**, *30*, 705–713. [CrossRef]
10. Zhang, Y.; Feng, X.; Zhang, X.; Wang, Z.; Sharifzadeh, M.; Yang, C. A novel application of strain energy for fracturing process analysis of hard rock under true triaxial compression. *Rock Mech. Rock Eng.* **2019**, *52*, 4257–4272. [CrossRef]
11. Li, T.; Yue, Z.; Li, J.; Chen, G.; Li, Q. Effect of confining pressure strength on the characteristics of energy evolution and fatigue fracture of the coal-rock structural body. *Fatigue Fract. Eng. Mater. Struct.* **2024**, *47*, 709–727. [CrossRef]
12. Du, X.; Xue, J.; Shi, Y.; Cao, C.; Shu, C.; Li, K. Triaxial mechanical behaviour and energy conversion characteristics of deep coal bodies under confining pressure. *Energy* **2023**, *266*, 126443. [CrossRef]
13. Li, S.; Wang, Z.; Wang, J.; Feng, C.; Li, A.; Wang, W. Failure characteristics and brittleness index establishment based on marble energy evolution mechanism. *Geomech. Energy Environ.* **2023**, *36*, 100504. [CrossRef]
14. Peng, R.; Ju, Y.; Wang, J.; Xie, H.; Gao, F.; Mao, L. Energy dissipation and release during coal failure under conventional triaxial compression. *Rock Mech. Rock Eng.* **2015**, *48*, 509–526. [CrossRef]
15. Miao, S.; Liu, Z.; Zhao, X.; Ma, L.; Zheng, Y.; Xia, D. Plastic and damage energy dissipation characteristics and damage evolution of Beishan granite under triaxial cyclic loading. *Int. J. Rock Mech. Min. Sci.* **2024**, *174*, 105644. [CrossRef]
16. Wang, C.; He, B.; Hou, X.; Li, J.; Liu, L. Stress–Energy Mechanism for Rock Failure Evolution Based on Damage Mechanics in Hard Rock. *Rock Mech. Rock Eng.* **2020**, *53*, 1021–1037. [CrossRef]
17. Wang, Y.; Cao, Z.; Mao, T.; Li, P.; Cai, M. Investigation of fatigue failure and energy characteristics of rock exposed to complicated stress disturbance paths: Cyclic stress amplitude effect. *Fatigue Fract. Eng. Mater. Struct.* **2023**, *46*, 2697–2713. [CrossRef]

18. Wu, Y.; Wang, Y.; Zhou, B.; Li, C.; Zhu, Y.; Sun, C.; Tian, Z. Study on the Deformation and Energy Evolution of Skarn With Marble Band of Different Orientations Under Cyclic Loading: A Lab-Scale Study. *Fatigue Fract. Eng. Mater. Struct.* **2024**, *47*, 4696–4713. [CrossRef]
19. Chu, Y.; Wang, M.; Song, S.; Zhang, J.; Zhang, D.; Liu, F. Experimental study on the mechanical properties, permeability characteristics, and energy evolution of gas-containing anthracite coal under different loading–unloading speeds. *Phys. Fluids* **2022**, *34*, 126608. [CrossRef]
20. Zhou, H.; Wang, X.; Zhang, L.; Zhong, J.; Wang, Z.; Rong, T. Permeability evolution of deep coal samples subjected to energy-based damage variable. *J. Nat. Gas Sci. Eng.* **2020**, *73*, 103070. [CrossRef]
21. Fu, J.; Li, B.; Ren, C.; Li, J.; Wang, Z.; Wu, X.; Jia, L. Coupling between Damage Evolution and Permeability Model with the Adsorption Effect for Coal under Gas Extraction and Coal Mining Conditions. *Energy Fuels* **2022**, *36*, 10813–10831. [CrossRef]
22. Wang, Z.; Li, B.; Ren, C.; Li, J.; Cheng, Q.; Wu, X. Energy-Driven Damage Constitutive Model of Water-Bearing Coal Under Triaxial Compression. *Rock Mech. Rock Eng.* **2024**, *57*, 1309–1328. [CrossRef]
23. Liu, D.; Guo, Y.; Li, J.; Lin, K. Damage constitutive model for layered yellow sandstone based on dissipative energy evolution and its verification. *Chin. J. Eng.* **2024**, *46*, 784–799. [CrossRef]
24. Guo, J.; Lu, X.; Yang, Q.; Jiang, J.; Chen, J.; Jiang, L. Establishment of rock strength criteria based on the elastic strain energy and its validation. *Chin. J. Rock Mech. Eng.* **2021**, *40*, 3147–3155. [CrossRef]
25. Yu, H.; Liu, S.; Jia, H.; Wang, S. Mechanical response and energy dissipation mechanism of closed single fractured sandstone under different confining pressures. *J. Min. Saf. Eng.* **2020**, *37*, 385–393. [CrossRef]
26. Wang, Z.; Zhao, W.; Pan, K. Analysis of fracture evolution characteristics of coplanar double fracture rock under uniaxial compression. *Geotech. Geol. Eng.* **2020**, *38*, 343–352. [CrossRef]
27. Wang, G.; Cao, T.; Sun, F.; Wen, X.; Zhang, L. Study on the Meso-Energy Damage Evolution Mechanism of Single-Joint Sandstone under Uniaxial and Biaxial Compression. *Adv. Mater. Sci. Eng.* **2021**, *2021*, 5245402. [CrossRef]
28. Wong, L.N.Y.; Li, H. Numerical study on coalescence of two pre-existing coplanar flaws in rock. *Int. J. Solids Struct.* **2013**, *50*, 3685–3706. [CrossRef]
29. Zhang, H.; Lu, C.; Liu, B.; Liu, Y.; Zhang, N.; Wang, H. Numerical investigation on crack development and energy evolution of stressed coal-rock combination. *Int. J. Rock Mech. Min. Sci.* **2020**, *133*, 104417. [CrossRef]
30. Chen, W.; Konietzky, H.; Tan, X.; Frühwirt, T. Pre-failure damage analysis for brittle rocks under triaxial compression. *Comput. Geotech.* **2016**, *74*, 45–55. [CrossRef]
31. Du, Y.; Li, T.; Li, W.; Ren, Y.; Wang, G.; He, P. Experimental study of mechanical and permeability behaviors during the failure of sandstone containing two preexisting fissures under triaxial compression. *Rock Mech. Rock Eng.* **2020**, *53*, 3673–3697. [CrossRef]
32. Zhu, W.; Gao, X.; Zhang, B.; Wu, Q. Laws of changes in the energy of gas hydrate-bearing coals under different confining pressures and saturation. *Coal Geol. Explor.* **2024**, *52*, 4. [CrossRef]
33. Li, B.; Zhang, Y.; Reng, C.; Yang, K.; Li, J.; Xu, J. Study on damage-energy evolution characteristics of coal under triaxial stress. *China Saf. Sci. J.* **2019**, *29*, 98–104. [CrossRef]
34. Zhang, A.; Xie, H.; Zhang, R.; Gao, M.; Xie, J.; Jia, Z.; Ren, L.; Zhang, Z. Mechanical properties and energy characteristics of coal at different depths under cyclic triaxial loading and unloading. *Int. J. Rock Mech. Min. Sci.* **2023**, *161*, 105271. [CrossRef]
35. Wang, Y.; Gao, S.; Li, C.; Han, J. Energy dissipation and damage evolution for dynamic fracture of marble subjected to freeze-thaw and multiple level compressive fatigue loading. *Int. J. Fatigue* **2021**, *142*, 105927. [CrossRef]
36. Gong, F.; Zhang, P.; Luo, S.; Li, J.; Huang, D. Theoretical damage characterisation and damage evolution process of intact rocks based on linear energy dissipation law under uniaxial compression. *Int. J. Rock Mech. Min. Sci.* **2021**, *146*, 104858. [CrossRef]
37. Chen, Z.; He, C.; Ma, G.; Xu, G.; Ma, C. Energy Damage Evolution Mechanism of Rock and Its Application to Brittleness Evaluation. *Rock Mech. Rock Eng.* **2019**, *52*, 1265–1274. [CrossRef]
38. Wang, L.; Liu, H.; Chen, L.; Liu, H.; Li, S.; Zhu, C.; Fan, H. Study on three-dimensional mesoscopic evolution characteristics and disturbance factors of coal open fractures. *Coal Sci. Technol.* **2024**, *52*, 71–83. [CrossRef]
39. Chen, M.; Zang, C.; Ding, Z.; Zhou, G.; Jiang, B.; Zhang, G.; Zhang, C. Effects of confining pressure on deformation failure behavior of jointed rock. *J. Cent. South Univ.* **2022**, *29*, 1305–1319. [CrossRef]
40. Ohtsu, M. *Acoustic Emission (AE) and Related Non-Destructive Evaluation (NDE) Techniques in the Fracture Mechanics of Concrete*; Woodhead Publishing: Cambridge, UK, 2021.